

# Understanding the Radiation Environment in Near-Earth Space and its Impact on the Earth's Atmosphere with Current and Future Space Missions

Robert A. Marshall <sup>1,2,3</sup>

1 University of Colorado Boulder, Boulder, CO, USA

2 Laboratoire de Physique et Chimie de l'Environnement et l'Espace (LPC2E), Orleans, France

3 LE STUDIUM Institute for Advanced Studies, 45000 Orléans, France

## REPORT INFO

*Fellow: Robert A. Marshall  
From University of Colorado Boulder  
Host laboratory in region Centre-Val de Loire: LPC2E  
Host scientist: Jean-Louis Pinçon  
Period of residence in region Centre-Val de Loire: January-July 2023*

### Keywords :

Space physics, radiation, radio waves, satellites

## ABSTRACT

*The Earth's radiation environment couples to the upper atmosphere through precipitation of energetic electrons in high-latitude regions. This precipitation is driven by electromagnetic waves in the plasma environment around the Earth, including waves generated by lightning discharges. We use data from the DEMETER mission, built and operated by LPC2E between 2004-2010, to better understand the propagation characteristics of these lightning-generated signals and their effects on the radiation environment. Further, we use lessons and heritage from the DEMETER mission to inform design decisions and data analysis techniques for the upcoming CANVAS mission, a collaboration between the University of Colorado Boulder and LPC2E. CANVAS is expected to launch in mid-2024.*

## 1- Introduction

A comprehensive description of Sun-Earth connections requires quantifying the solar and magnetospheric energy input to the atmosphere. The energy from Energetic Particle Precipitation (EPP) leads initially to the production of reactive odd nitrogen ( $\text{NO}_x = \text{N} + \text{NO} + \text{NO}_2$ ) (Rusch et al, 1981) and odd hydrogen ( $\text{HO}_x = \text{H} + \text{OH} + \text{HO}_2$ ) (Solomon et al, 1981), both of which catalytically destroy ozone, a radiatively active gas. Through various dynamical and chemical processes, the absorbed energy is redistributed, and its effects amplified through such mechanisms as catalytic cycles and nonlinear wave/mean-flow interactions. Thus, EPP plays a critical role in driving the chemistry and potentially the radiative balance and circulation of the atmosphere.

VLF waves play an important role in controlling the evolution of energetic electron distributions

in near-Earth space. Whistler-mode waves propagating in the magnetospheric plasma can induce pitch-angle scattering and precipitation of trapped energetic particles (e.g., Imhof et al, 1983, Inan et al 1987). Abel and Thorne (1998) concluded that both VLF waves radiated from lightning and ground-based VLF transmitters play a significant role in maintaining the slot region of depleted fluxes between the inner and outer radiation belts. However, an accurate quantification of the amount of VLF energy which penetrates from the ground, through the ionosphere, and into the magnetosphere is critical to these conclusions (e.g., Inan et al 2010), together with an understanding of the propagation characteristics of these waves as they traverse the ionosphere and magnetosphere. The key characteristics of these upward-propagating waves are thus i) their amplitude above the ionosphere, and the spatial distribution of that amplitude; and ii) the propagation direction above the ionosphere,

captured by the wave normal angle (WNA), which is the angle between the wave direction of phase propagation (the  $k$ -vector) and the background magnetic field.

The wave amplitudes above the ionosphere have received the most attention, both analytically and through observations. However, despite the fact that quantitative estimates of trans-ionospheric attenuation of VLF waves are important for many studies in space sciences, most prior studies (e.g., Abel and Thorne 1998, Bortnik et al 2003, Starks et al 2008) have relied on absorption curves given by Figure 3-35 of Helliwell (1965). These trans-ionospheric absorption estimates were presented at the time with several known caveats, and recent in situ satellite observations (e.g., Starks et al 2008) have shown some significant disagreement. Helliwell presented the total trans-ionospheric absorption of a whistler through the ionosphere as a function of frequency, geomagnetic latitude, and day vs. night conditions. These curves were originally intended only for mid-latitude and high-latitude analysis of whistler-mode waves incident upon the ionosphere with wave normal angles (WNAs) that are able to reach the ground. Starks et al (2008) used the Air Force Research Laboratory's VLF Propagation Code to produce a three-dimensional model for illumination of the plasmasphere by terrestrial VLF transmitters. They then compared the model to measurements from dozens of DEMETER satellite passes over several VLF transmitters, and concluded that Helliwell's profiles underestimate the 20 kHz mid-latitude attenuation by about 10 dB in daytime and 20 dB at night. Tao and Bortnik (2010) applied an electromagnetic full wave method for trans-ionospheric absorption and analyzed D-region electron density variation; their results suggested that even more discrepancy (up to 100 dB) may be present when using more realistic electron density profiles.

Cohen et al (2012a,b) provided the first consistent agreement between satellite-based observations and modeling results of the amplitudes above terrestrial VLF transmitters. Cohen et al (2012a) analyzed thousands of DEMETER satellite passes over a dozen VLF

transmitters to provide pass-averaged radiation maps at 700 km altitude. From these maps, the total power injected into the magnetosphere from each transmitter was calculated for both daytime and nighttime. Cohen et al (2012b) then compared these power estimates to the results of a full wave method (FWM) model described by Lehtinen and Inan (2008). Results showed very good agreement between the model and data, to within 6 dB for both daytime and nighttime for every transmitter considered.

Most recently, Graf et al (2013) generated trans-ionospheric attenuation curves using the FWM model of Lehtinen and Inan (2008) and compared the results to the Helliwell curves. Both Helliwell and Graf predict significantly more attenuation at lower latitudes, but the effect is less pronounced in the FWM results; in comparison to Helliwell, Graf predicts less attenuation at low latitudes and more attenuation at high latitudes; however the two models agree to within 5 to 10 dB under most conditions.

While the *Cohen* and *Graf* results show improved agreement between models and data, they lack a number of key inputs. First, the model-data comparison from Cohen is done only for transmitters, and not over the broadband emissions of lightning. The Graf modeling results provide trans-ionospheric attenuation curves for any frequency, but require validation with broadband observations of lightning. Addressing these deficiencies is one of the primary goals of the project described herein.

Figure 1 shows an example output from the FWM, simulating a single frequency of 19.8 kHz. The top panel shows electric field amplitude, in Volts per meter (V/m), in the  $x$ - $z$  plane. The lower left panel shows the angle between the magnetic field ( $B_{geo}$ ) and the direction of energy propagation ( $S$ ) at 500 km altitude, i.e. above the atmosphere and ionosphere, while the lower right panel shows the angle between the magnetic field and the direction of phase propagation ( $k$ ). Both of these angles are crucial for understanding propagation through the ionosphere and into the magnetosphere. Previous work has assumed

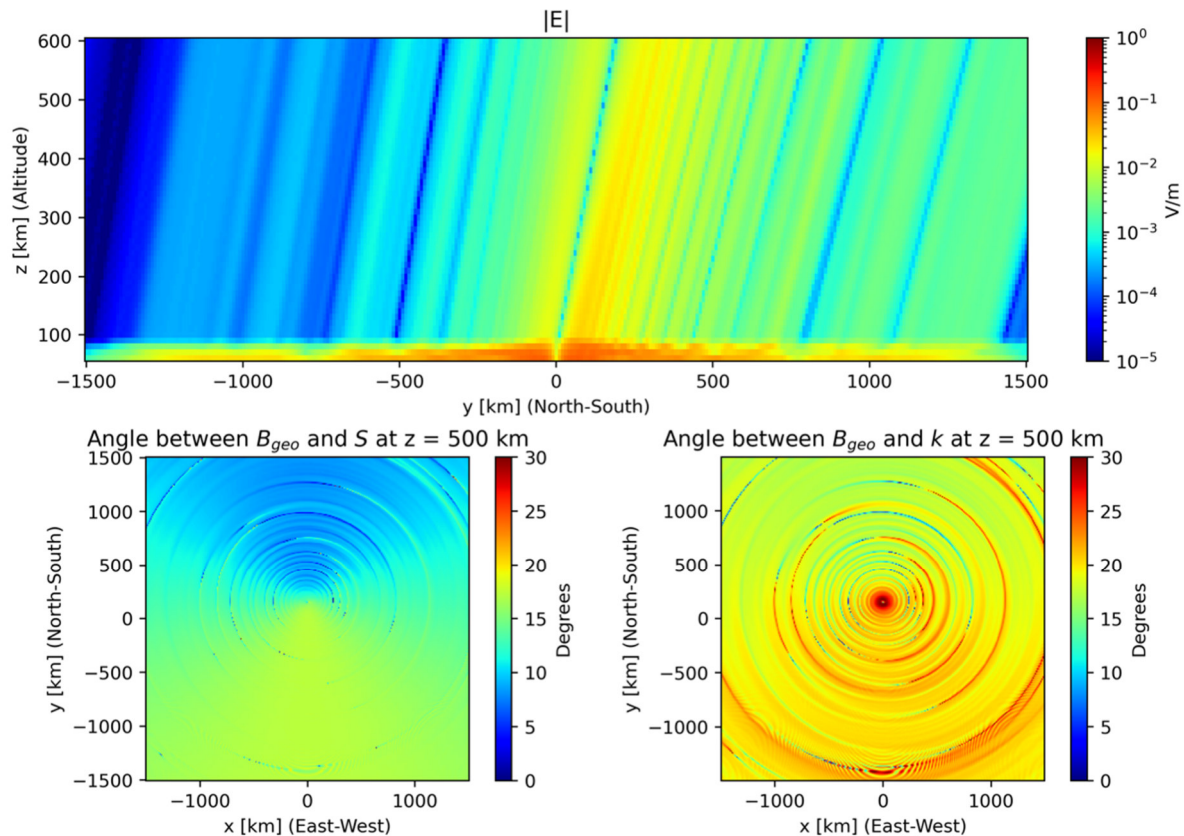


Figure 1: Full-wave model (FWM) simulation at 19.8 kHz, showing the electric field magnitude (top), Poynting vector angle (lower left), and wave normal angle (WNA, lower right).

that the angle between  $B_{geo}$  and  $S$  is zero, i.e. energy flows along the magnetic field lines; but these simulations show that that is not the case. One of the goals of this work, and of the CANVAS mission, is to improve our understanding of these characteristics of wave propagation, and to validate this numerical modeling with observations above the ionosphere.

## 2- Experimental details

The DEMETER mission (Parrot, 2002) was launched in 2004 with the primary goal of studying radio emissions associated with earthquakes. However, secondary goals were developed to study lightning-generated whistlers and VLF transmitters, because the instruments on board the spacecraft were very well suited to such studies. There had been very few observations of VLF waves in low-Earth orbit prior to DEMETER, so it turned out to be quite a unique and important mission for this community.

The key instruments for this study include the Instrument Magnetic Search Coil (IMSC) and the Instrument Champ Electrique (ICE), which measure magnetic and electric components of VLF waves, respectively (Parrot et al, 2006; Berthelier et al 2006). The IMSC consisted of a three-axis search coil system as well as associated electronics, and provides the heritage and precursor sensors to CANVAS. The three-axis search coil was deployed on a 1.9 meter boom to isolate the very sensitive search coils from spacecraft noise. The ICE instrument was a three-axis electric field instrument using four 4-meter stacer booms with small conducting spheres at the ends. Pairs of these antennas are used to measure the electric field components in each of the three cardinal axes. While ICE can measure from DC to 3 MHz, the IMSC can only measure from about 100 Hz to 20 kHz, due to well-known limitations of search coil magnetometers. For the purposes of this study, we restrict our analysis for both instruments from DC to 20 kHz, as those are the most important frequencies for lightning and VLF

transmitter signals observed above the ionosphere.

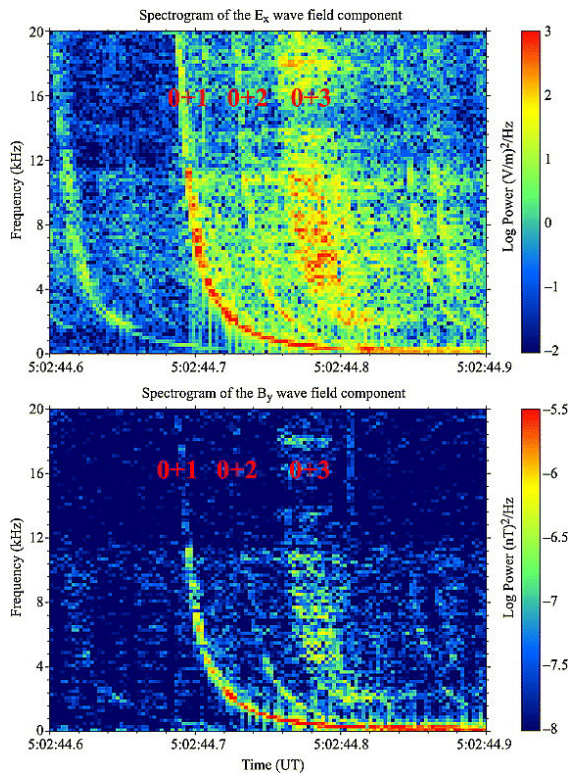


Figure 2: Example lightning-generated whistler observed on the DEMETER satellite, in electric field (top) and magnetic field (bottom).

Figure 2 shows an example 0+ whistler (i.e., on its initial upward trajectory) recorded by the DEMETER spacecraft; this event was analyzed by Lefeuvre et al (2009) in conjunction with ground-based VLF observations of the source lightning flash. The top panel shows the electric field signal; the lower panel shows the magnetic field signal. This example whistler shows that these events span about 200 ms due to their dispersion (lower frequencies propagate slower in the ionospheric plasma), but the duration of any particular frequency component is brief, less than about 10 ms (limited here by the time resolution of the spectrogram). Since the goal of the upcoming CANVAS mission is to measure the total VLF energy, it will sample with a longer time resolution of 1 second. This time resolution is sufficient for the science goals while also meeting the spacecraft data budget.

Figure 2 shows the electric and magnetic field amplitudes of a whistler, but more important are the energy flux and propagation direction, which is given by  $k$ , the wave normal vector.

The angle between  $k$  and the Earth’s magnetic field  $B$  is called the wave normal angle or WNA. This angle determines how the VLF energy propagates and the trajectory it takes into the magnetosphere.

From five channels of VLF data, Santolik et al (2003) describe the method for calculating WNA, along with other wave parameters such as polarization, ellipticity, planarity, and more. The underlying assumption in the method is that the wavefront is planar, and this assumption is verified with the method’s estimate of wave planarity.

The Santolik method can operate with three magnetic field components, or with magnetic and electric field components. From the raw, time-domain data, we calculate frequency-domain components with user-defined time and frequency resolution; in this work we use a time step of 50 ms, and a frequency step of 10 Hz. Next, we calculate the spectra and cross-spectra of the field components, i.e.  $S_{ij} = B_i B_j^*$ , where  $i, j$ , and  $k$  represent the  $x, y$ , and  $z$  components of the magnetic field, and  $*$  is the complex conjugate. From the real and imaginary parts of these spectral matrix components, we generate the  $A$  matrix defined in Santolik:

$$A = \begin{bmatrix} \Re S_{11} & \Re S_{12} & \Re S_{13} \\ \Re S_{12} & \Re S_{22} & \Re S_{23} \\ \Re S_{13} & \Re S_{23} & \Re S_{33} \\ 0 & -\Im S_{12} & -\Im S_{13} \\ \Im S_{12} & 0 & -\Im S_{23} \\ \Im S_{13} & \Im S_{23} & 0 \end{bmatrix}$$

Where script “R” represents the real part of  $S$ , and script “I” represents the imaginary part. The subscripts 1, 2, 3 represent the  $x, y$ , and  $z$  components of the field components that go into the calculation of  $S$ , as defined above. Next, the matrix  $A$  is decomposed using singular value decomposition:

$$[U, s, V^T] = \text{svd}(A)$$

In this factorization, the vector  $s$  provides the parameters for the polarization and planarity of the wave, while  $V^T$  can be used to evaluate the wave normal angle.

We have applied this method to burst-mode ELF data from the DEMETER mission. While DEMETER VLF data has only one channel in burst mode, ELF data includes all channels, but for frequencies only up to 1.2 kHz. We have used 18 samples of burst-mode DEMETER ELF data in order to adjust and validate the methodology and ensure its robustness. Future work will apply the analysis to the full 6-year DEMETER dataset, which includes thousands of burst events.

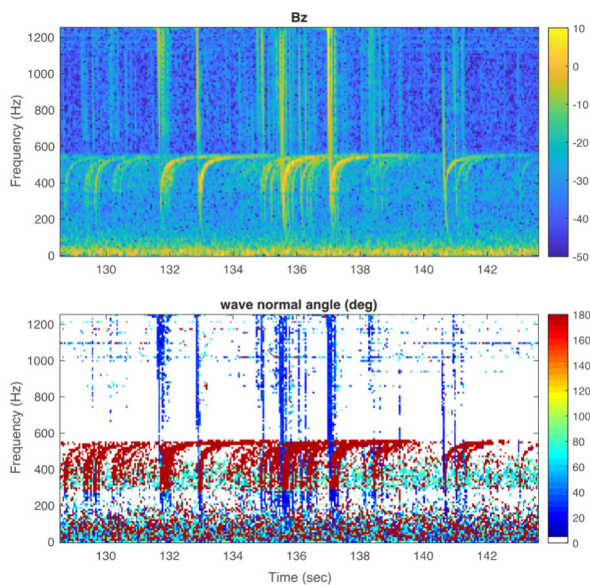


Figure 3: Example whistler data processed to calculate WNA. Top panel shows Bz component; other components are not shown for brevity.

Figure 3 shows an example where our data processing technique has been applied to DEMETER data. This example shows ~14 seconds of data, which includes numerous whistlers, but we use this case to focus on the most prominent handful of whistlers.

The top panel of Figure 3 shows the z-component of the magnetic field (Bz); the other components are omitted for brevity. The vertical lines above ~600 Hz are electron whistlers from lightning; the hooked lines below 600 Hz are proton whistlers generated by the same lightning discharges. These are waves where the primary controlling force is the response of protons to the wave fields, rather than electrons; because protons are 2000 times heavier than electrons, they respond at much lower frequencies. The cutoff frequency around 600 Hz represents the proton cyclotron frequency. It is well known that the group velocity of whistler waves approaches zero at the cyclotron frequency; as such, wave components near the cyclotron frequency take considerably longer to reach the spacecraft.

The WNA analysis of this event is shown in the lower panel of Figure 3. This panel shows the calculated wave normal angles for the entire 14-second period in frequency space. The electron whistlers appear blue, evidence of WNAs near zero degrees; these waves are therefore propagating along the Earth’s magnetic field, as expected, with right-hand circular polarization. The proton whistlers appear red, with WNAs near 180 degrees; they are also parallel to Earth’s magnetic field, but with left-hand circular polarization, which appears in this analysis as an inverted propagation direction. These results confirm that the analysis is producing the expected results.

Also of interest in Figure 3 is the cyan signature at about 400 Hz that appears “behind” the proton whistlers. This is likely evidence of

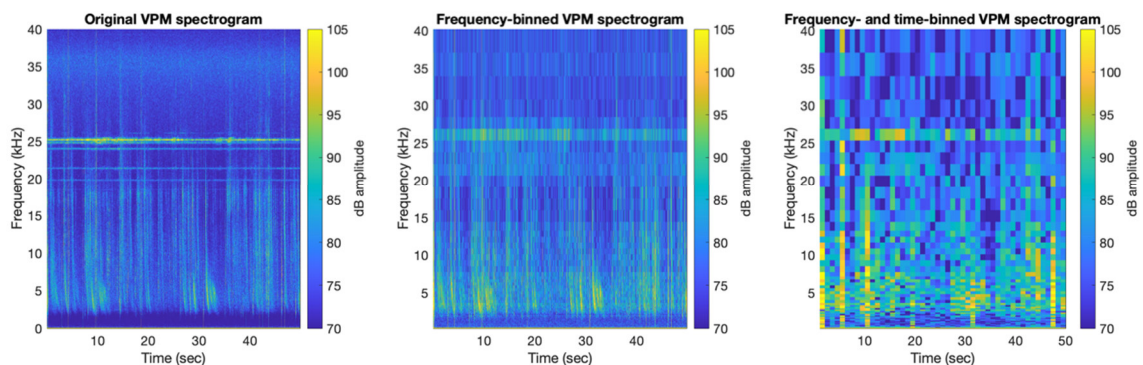


Figure 4: VPM data processed with CANVAS reduction algorithm to emulate expected signals.

plasmaspheric hiss, a type of VLF wave naturally generated in the space environment. The cyan color shows that its WNA is near 90-degrees, i.e. propagating with a k-vector perpendicular to the magnetic field. As such, this analysis is able to extract wave components from the raw VLF data that are not otherwise evident (such as in Figure 3, top panel).

These results are just the beginning of DEMETER ELF analysis. With the method in hand, we will apply this analysis to the full six-year DEMETER dataset, creating a statistical picture of DEMETER whistler signals and their wave normal angles. However, more immediately, these results pave the way for the CANVAS mission, and interpretation of the VLF dataset that will result.

### 3- The CANVAS mission

DEMETER made invaluable observations of VLF waves above the ionosphere at ~700 km altitude; however, the mission was not designed with this goal, and was limited to VLF observations in burst mode over specific regions of the globe, and with only one channel each (electric and magnetic) collecting full-resolution data. Furthermore, DEMETER operated in a sun-synchronous orbit, and sampled only 10:30 and 22:30 local times; and there was no global lightning geolocation data during its mission (the GLD360 network began operation in 2013). The upcoming CANVAS mission is designed to follow in DEMETER's footsteps, while overcoming some of the gaps as they relate to lightning and transmitter VLF emissions. CANVAS' orbit will ensure continuous observations of VLF waves and will cover all local times throughout its one-year mission, in order to provide a complete climatology of VLF energy injected into the space environment.

The primary goal of the CANVAS mission is to estimate the energy flux from lightning and VLF transmitters that is injected into the magnetosphere. We will make this estimate for individual events, but also as a global, climatological estimate, useful for global climate modeling. To achieve these goals, the CANVAS CubeSat (Figure 5) includes a two-

axis electric field antenna system, and a three-axis magnetic search coil antenna system. With five of the possible six components measured, we can estimate the Poynting (i.e. energy) flux and its direction, as well as the WNA, for each event observed. These parameters will enable modelers to estimate the distribution of that energy within the magnetosphere, and its

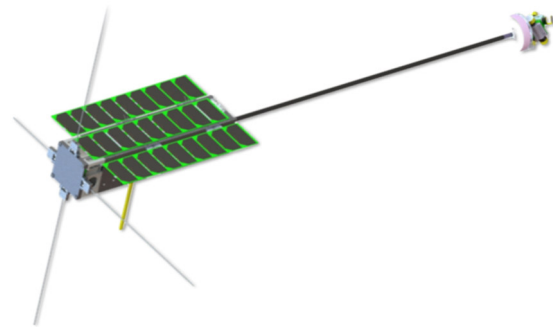


Figure 5: CANVAS CubeSat, showing deployed electric field antennas (left) and deployed search coil system (far right)

interactions with radiation belt particles.

CANVAS will record data at full resolution (16 bit sampling,  $2^{17}$  samples per second on each channel); but the raw 130 GB per day are far too much data to bring to the ground. Therefore, onboard processing in an FPGA reduces the data volume to 200 MB per day by compressing in time and frequency space. To demonstrate the compression on real spacecraft data, we have developed the code to apply the same compressions to data from the VLF Precipitation Mapper (VPM) CubeSat, a mission launched in 2020 with one electric field dipole antenna and one search coil, also built by LPC2E. Unfortunately the search coil on that mission failed to deploy, so only the electric field data was usable.

Figure 4 shows the result of applying the CANVAS compression to VPM data. The leftmost panel is the raw VPM data, processed into a time-frequency spectrogram, to show the different frequency components of the signal. The spectrogram data is then binned in frequency space using 57 log-spaced frequency bins, with the result shown in the middle panel. After also binning in time to 1-second resolution, the final result is shown on the right. While the most prominent whistlers are still

evident, it is clear that with this data compression method we will not be able to discern each individual whistler. Not shown, ten individual frequencies are saved separately at high resolution in order to monitor the major ground-based VLF transmitters.

#### 4- CANVAS Preparation : E-field

A model of the CANVAS electric field instrument is shown in Figure 6. The aluminum base forms one face of the spacecraft, while the electric field preamplifier (green) is designed to sit underneath that panel. Four antennas deploy from the panel with custom-designed hinges, and the signal from the antenna is routed through the panel to the preamplifier. The antenna and hinge must be carefully designed to avoid stray capacitance, while ensuring no charge builds up on external surfaces that could cause arcing while operating in the plasma of the ionosphere.

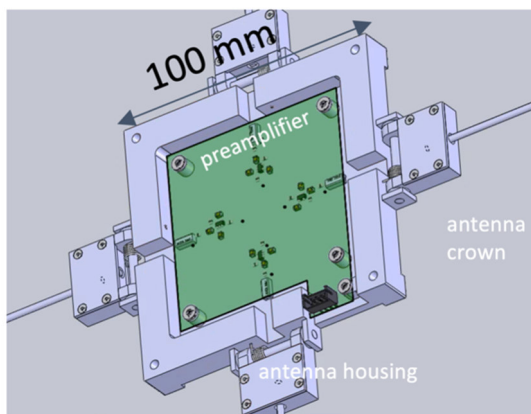


Figure 6: CANVAS electric field antenna system, showing the embedded preamplifier board and deployment hinge housings

The CANVAS electric field instrument consists of four 40-cm monopole antennas, which together make two dipoles in orthogonal axes. The preamplifiers circuits, intergrated into the spacecraft top panel, are simple buffers, providing a low impedance output to the analog receiver. The analog receiver provides amplification and anti-alias filtering before passing the signal to an ADC.

The CANVAS electric field instrument has been built and tested at CU Boulder over the past year. Testing and characterization has been conducted and results analyzed in consultation

with LPC2E colleagues to ensure that the system will meet CANVAS' measurement requirements. Figure 7 shows the measured sensitivity of the electric field instrument, in units of  $\mu\text{V}/\text{m}/\text{rt-Hz}$ . The nominal science requirement for the CANVAS mission is a sensitivity of  $1 \mu\text{V}/\text{m}/\text{rt-Hz}$ , shown with the horizontal dashed line. Thus we see that the instrument meets or exceeds the sensitivity requirement at all frequencies of interest.

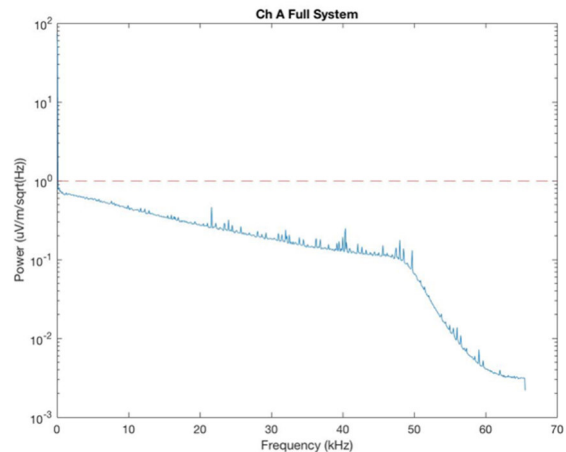


Figure 7: Sensitivity of the E-field instrument, well below the requirement shown with the dashed line.

Figure 8 shows some the frequency response (i.e. the gain) of the complete electric field instrument, from the antenna to digital data conversion. The frequency response shows the high-pass filter at 300 Hz, used to eliminated the DC component of the electric field, and the low-pass filter at 40 kHz, used to prevent aliasing of higher-frequency signals. The instrument performance matches the design goals and meets the requirements for flight.

#### 5- CANVAS Preparation : B-field

The magnetic field instrument of CANVAS was designed with closer consultation and collaboration with LPC2E when compared to the electric field instrument. The magnetic search coils themselves were built by LPC2E, and the preamplifier was built using the DEMETER design specifications provided by LPC2E. The preamplifier circuit provides most of the signal gain, since the output from the search coils themselves is a very small voltage. The rest of the gain is applied in the analog

receiver; the remainder of the analog electronics are identical to the electric field channels.

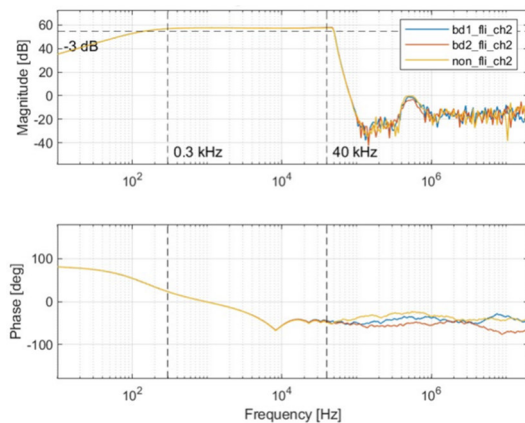


Figure 8: CANVAS E-field instrument frequency response, showing amplitude (top) and phase (bottom) response, together with the requirements shown as dashed lines.

DEMETER informs the requirements for the search coil design and performance, since it used similar search coils in a near-identical orbit. The DEMETER search coils thus informed the expected signal strength in orbit, and thus the gain required in the electronics. The CANVAS search coils are slightly shorter than DEMETER's, in order to fit inside the CubeSat structure. To enhance the instrument sensitivity in the reduced form factor, flux concentrators were added to the ends of the search coils, as shown in Figure 9.

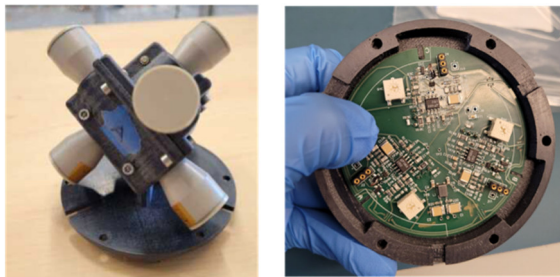


Figure 9: CANVAS magnetic field search coil system, with 3D-printed holder and embedded preamplifier board

The estimation of WNAs from the data is limited by the crosstalk between channels. For example, if 1% of the signal of the x-component also appears on the y-component, then the WNA can only be estimated to about 1 degree accuracy. Crosstalk is reduced if the coil centers are as close as possible to each other. Thus, LPC2E designed barbell-shaped housings for the search coils, as shown in Figure XX.

Measurements of crosstalk have so far yielded a worst-case of 25 dB, which yields WNA uncertainty of 3 degrees. Ongoing work is being conducted to improve the assessment of the crosstalk, which is limited by the capabilities of the testing facilities.

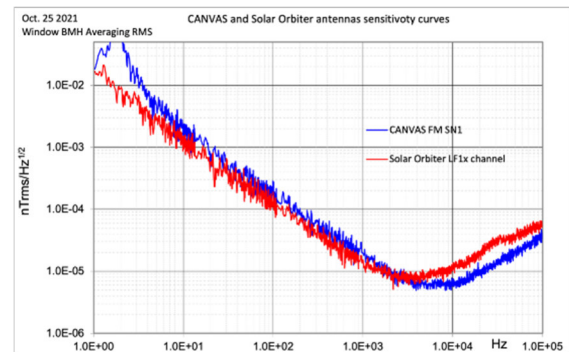


Figure 10: Search coil sensitivity for CANVAS (blue) and the much larger and more expensive Solar Orbiter mission (red).

Figure 10 shows the measured sensitivity of the CANVAS search coils, along with the frequency response for the search coils on the much larger Solar Orbiter mission; LPC2E built the complete search coil instrument for that mission, with very similar search coils. Despite their small size, the search coils nearly match the performance of the Solar Orbiter instrument, on a much larger and more expensive mission. The frequency response was intentionally shifted towards higher frequencies (i.e. to the right) for CANVAS in order to capture the higher-frequency components of lightning-generated whistlers.

## 6- Conclusion

In this project we have analyzed ELF data from the DEMETER mission to assess wave normal angles (WNAs) of lightning-generated whistlers. The DEMETER dataset has been used to inform the design and characterization of the instruments onboard the CANVAS CubeSat. The electric field instrument design and characterization has benefitted from consultation by LPC2E colleagues, but the magnetic search coil instrument has relied on LPC2E design greatly. Design improvements have let to CANVAS search coils with performance that rivals those on Solar Orbiter, a much larger mission.

The CANVAS mission is expected to launch in the first half of 2024. The DEMETER data analysis has provided the tools necessary to conduct data analysis once CANVAS is in space. The CANVAS instrument design and characterization, under collaboration with LPC2E, has yielded instruments that will make measurements with high performance

#### **7- Perspectives of future collaborations with the host laboratory**

The analysis of DEMETER data that began in this work is ongoing. The code has been developed to analyze the full six-year dataset; that work will continue in the next year. We plan to build a statistical dataset of whistlers from DEMETER, and use those to study the propagation characteristics through the ionosphere. While CANVAS will be best suited for this work in VLF frequencies, because CANVAS cannot measure below 300 Hz, DEMETER data can complement those studies using its ELF data, as shown in Figure 3. Those observations are particularly interesting for the study of proton whistlers, as discussed earlier, and thereby the proton densities in the ionosphere.

The collaboration on CANVAS search coils has been especially fruitful. Through this fellowship, a transfer of knowledge has occurred in two directions: search coil information from LPC2E to the author, and CubeSat design and testing information from the author to LPC2E. As LPC2E works towards integrating their own instruments on CubeSats in the future, collaboration and consultation with the author will continue. LPC2E will also participate in CANVAS data analysis.

The author is the instrument PI on a proposed NASA mission that will fly four spacecraft in the radiation belts, each carrying a three-axis search coil. With engineering models and flight spares, this mission will require 21 search coils to be designed, built, and tested, along with their preamplifiers and analog receiver electronics. LPC2E has committed to supporting the design of these search coils, but the work will be conducted at CU Boulder. This collaboration will help bring a new instrument capability to

CU Boulder and the author's laboratory. LPC2E will remain involved in that mission, including science and data analysis.

#### **8- Articles published in the framework of the fellowship**

The work conducted in this visiting researcher fellowship has been included in the following talks and presentations over the past six months:

1. Marshall, R. A., Imaging Energetic Particle Precipitation into Earth's Upper Atmosphere through Backscattered Hard X-rays; *invited* seminar for the Birkeland Center for Space Science, University of Bergen, Bergen, Norway; March 20, 2023.
2. Marshall, R. A., Lightning-induced Electron Precipitation and its indirect effects on the upper atmosphere, *invited* seminar at LPC2E, Orleans, France, March 14, 2023.
3. Marshall, R.A., Direct and indirect effects of the lightning EMP on the mesosphere and lower ionosphere; *invited* presentation at *Radio Observations and Theory of Atmospheric Discharge Processes* workshop, Bath, UK, June 28, 2023.
4. Marshall, R. A., D. M. Malaspina, T. Dudok de Wit, G. Jannet, J. M. Cannon, M. Stratton, and S. Wankmueller, Design and Performance of the Compact Five-channel VLF Wave Receiver on the CANVAS CubeSat Mission; presented at URSI General Assembly, Sapporo, Japan, August 24, 2023.

No journal publications have yet been submitted; however, a publication on the CANVAS instrument design is in preparation, and another publication will be written on the spacecraft and mission design. These papers will be submitted shortly after the mission launches to space.

#### **9- Acknowledgements**

The author wishes to acknowledge Le Studium for the opportunity to conduct this Visiting Researcher fellowship in Orléans in collaboration with LPC2E colleagues. The CANVAS mission development is funded by

the US National Science Foundation under grant number AGS1841011.

## 10- References

- Abel, B., & Thorne, R. M. (1998). Electron scattering loss in earth's inner magnetosphere: 1. dominant physical processes. *Journal of Geophysical Research: Space Physics*, 103(A2), 2385–2396.
- Bortnik, J., Inan, U. S., & Bell, T. F. (2003). Energy distribution and lifetime of magnetospherically reflecting whistlers in the plasmasphere. *J. Geophys. Res.*, 108(A5), 1199.
- Cohen, M. B., & Inan, U. S. (2012). Terrestrial vlf transmitter injection into the magnetosphere. *J. Geophys. Res.*, 117, A08310.
- Cohen, M. B., Lehtinen, N. G., & Inan, U. S. (2012). Models of ionospheric VLF absorption of powerful ground based transmitters. *Geophys. Res. Lett.*, 39, L24101.
- Graf, K. L., Spasojevic, M., Marshall, R. A., Lehtinen, N. G., Foust, F. R., & Inan, U. S. (2013). Extended lateral heating of the nighttime ionosphere by ground-based vlf transmitters. *J. Geophys. Res.*, 118(12), 7783-7797.
- Helliwell, R. A. (1965). *Whistlers and related ionospheric phenomena*. Stanford University Press.
- Imhof, W. L., Reagan, J. B., Voss, H. D., Gaines, E. E., Datlowe, D. W., Mobilia, J., . . . Joiner, R. G. (1983). Direct observation of radiation belt electrons precipitated by the controlled injection of VLF signals from a ground-based transmitter. *Geophys. Res. Lett.*, 10, 361-364.
- Inan, U. S., & Carpenter, D. L. (1987). Lightning-induced electron precipitation events observed at L=2.4 as phase and amplitude perturbations on subionospheric VLF signals. *J. Geophys. Res.*, 92(A4), 3293-3303.
- Inan, U. S., Cummer, S. A., & Marshall, R. A. (2010). A survey of ELF and VLF research on lightning-ionosphere interactions and causative discharges. *J. Geophys. Res.*, 115, A00E36.
- Lefeuvre, F., Marshall, R., Pincon, J. L., Inan, U. S., Lagoutte, D., Parrot, M., & Berthelier, J.-J. (2009). On remote sensing of transient luminous events' parent lightning discharges by ELF/VLF wave measurements on board a satellite. *J. Geophys. Res.* 114, A09303.
- Lehtinen, N. G., & Inan, U. S. (2008). Radiation of ELF/VLF waves by harmonically varying currents into a stratified ionosphere with application to radiation by a modulated electrojet. *J. Geophys. Res.*, 113, A06301.
- Rusch, D., Gerard, J.-C., Solomon, S., Crutzen, P., & Reid, G. (1981). The effect of particle precipitation events on the neutral and ion chemistry of the middle atmosphere—i. odd nitrogen. *Planetary and Space Science*, 29(7), 767–774.
- Santolik, O., Parrot, M., & Lefeuvre, F. (2003). Singular value decomposition methods for wave propagation analysis. *Radio Science*, 38(1).
- Solomon, S., Reid, G. C., Roble, R. G., & Crutzen, P. J. (1982). Photochemical coupling between the thermosphere and the lower atmosphere: 2. d region ion chemistry and the winter anomaly. *J. Geophys. Res.*, 87(C9), 7221-7227.
- Starks, M. J., Quinn, R. A., Ginet, G. P., Albert, J. M., Sales, G. S., Reinisch, B. W., & Song, P. (2008). Illumination of the plasmasphere by terrestrial very low frequency transmitters: Model validation. *J. Geophys. Res.*, 113, A09320.
- Tao, X., Bortnik, J., & Friedrich, M. (2010). Variance of transionospheric vlf wave power absorption. *J. Geophys. Res.*, 115, A07303.